Cellular/Molecular

Presynaptic Calcium Stores Modulate Afferent Release in Vestibular Hair Cells

Andrea Lelli,[1,4] Paola Perin,[2] Marta Martini,[3] Catalin D. Ciubotaru,[1,4] Ivo Prigioni,[2] Paolo Valli,[2] Maria L. Rossi,[3] and Fabio Mammano[1,4,5]

[1]Venetian Institute of Molecular Medicine, via Giuseppe Orus 2, 35129 Padua, Italy, [2]Department of Cell and Molecular Physiological and Pharmacological Sciences, University of Pavia, via Forlanini 6, 27100 Pavia, Italy, [3]Department of Biology, Section of Physiology and Biophysics and Center for Neurosciences, University of Ferrara, via Borsari 46, 44100 Ferrara, Italy, [4]National Institute of Physics of Matter, and [5]Department of Physics, University of Padua, via Marzolo 8, 35129 Padua, Italy

Hair cells, the mechanoreceptors of the acoustic and vestibular system, are presynaptic to primary afferent neurons of the eighth nerve and excite neural activity by the release of glutamate. In the present work, the role played by intracellular Ca^{2+} stores in afferent transmission was investigated, at the presynaptic level, by monitoring changes in the intracellular Ca^{2+} concentration ($[Ca^{2+}]_i$) in vestibular hair cells, and, at the postsynaptic level, by recording from single posterior canal afferent fibers. Application of 1–10 mM caffeine to hair cells potentiated Ca^{2+} responses evoked by depolarization at selected Ca^{2+} hot spots, and also induced a graded increase in cell membrane capacitance (ΔC_m), signaling exocytosis of the transmitter. Ca^{2+} signals evoked by caffeine peaked in a region located ~10 μm from the base of the hair cell. $[Ca^{2+}]_i$ increases, similarly localized, were observed after 500 msec depolarizations, but not with 50 msec depolarizations, suggesting the occurrence of calcium-induced calcium release (CICR) from the same stores. Both Ca^{2+} and ΔC_m responses were inhibited after incubation with ryanodine (40 μM) for 8–10 min. Consistent with these results, afferent transmission was potentiated by caffeine and inhibited by ryanodine both at the level of action potentials and of miniature EPSPs (mEPSPs). Neither caffeine nor ryanodine affected the shape and amplitude of mEPSPs, indicating that both drugs acted at the presynaptic level. These results strongly suggest that endogenous modulators of the CICR process will affect afferent activity elicited by mechanical stimuli in the physiological frequency range.

Key words: **calcium-induced calcium release; ryanodine receptor; exocytosis; voltage-activated Ca^{2+} channels; calcium hot spots; labyrinth; frog; synapse; afferent discharge; patch clamp; fluorescence microscopy**

Introduction

Calcium-induced calcium release (CICR) is an amplification process whereby the increase of $[Ca^{2+}]_i$ mediated by the opening of Ca^{2+}-permeable channels activates Ca^{2+} release from intracellular stores (Endo et al., 1970). CICR depends on a caffeine- and ryanodine-sensitive Ca^{2+} channel, the ryanodine receptor (RyR), present on the membrane of endoplasmic and sarcoplasmic reticulum (Meldolesi and Pozzan 1998; Williams, 2002). Three isoforms of RyR are known, which are differentially expressed in muscular tissues but are all found in neurons (Sorrentino, 2003). Together with inositol triphosphate (IP_3) receptors, RyRs have been implicated in the modulation of neuronal synaptic transmission (Berridge, 1998; Rose and Konnerth, 2001). CICR is thought to enhance evoked exocytosis in frog motor nerve terminals (Narita et al., 2000) and to shape the presynaptic Ca^{2+} response at basket cell–Purkinje cell synapses (Llano et al., 2000) and presynaptic terminals of pyramidal neurons in hippocampal slice cultures (Emptage et al., 2001; but see also Carter et al., 2002).

The rate of transmitter release at the synapse between the hair cell and the afferent terminal (cytoneural junction) is modulated by changes of the cell membrane potential (Parsons et al., 1994; Moser and Beutner, 2000). Unlike most neurons, the hair cells of auditory and vestibular epithelia produce graded membrane potential changes (receptor potentials) in response to mechanical stimulation of the hair bundle, which alters the open probability of voltage-dependent Ca^{2+} channels clustered at presynaptic active zones (Roberts et al., 1990; Fuchs, 2002).

Fluorescence imaging with Ca^{2+}-selective dyes shows that depolarization elicits Ca^{2+} entry at selected hot spots at the basal (synaptic) pole of hair cells from the frog semicircular canal (Rispoli et al., 2001; Martini et al., 2002), most likely corresponding to clusters of voltage-gated Ca^{2+} channels (Rodriguez-Contreras and Yamoah, 2001). Similar hot spots have been described in other types of hair cells (Tucker and Fettiplace, 1995; Issa and Hudspeth, 1996, Ricci et al., 2000).

Data suggesting the occurrence of CICR processes in hair cells

Received Feb. 28, 2003; revised May 29, 2003; accepted June 9, 2003.

This work was supported by grants from Centro di Eccellenza dell'Università di Padova to Professor Tullio Pozzan (coordinator), Istituto Nazionale di Fisica della Materia (Section B2, Trieste Unit) (F.M.), and Ministero dell'Università e della Ricerca Scientifica e Tecnologica (F.M., P.V., I.P., M.L.R.). C.D.C. was supported by a United Nations Industrial Development Organization Fellowship. We thank Prof. Riccardo Fesce for many helpful comments on this manuscript.

Correspondence should be addressed to Dr. Fabio Mammano, Istituto Veneto di Medicina Molecolare, via Giuseppe Orus, 2, 35129 Padua, Italy. E-mail: fabio.mammano@unipd.it.

 0270-6474/03/236894-10$15.00/0

have been published recently (Evans et al., 2000, Glowatzki and Fuchs, 2002; Kennedy and Meech, 2002), although conclusive evidence is still lacking. In particular, the link between CICR and neurotransmitter release at hair cell afferent synapses has been postulated but not demonstrated, and the structures involved have not been identified in acoustic or vestibular systems. In the present work, we investigated CICR and its effects on afferent synaptic transmission by simultaneously monitoring hair cell ΔC_m and $[Ca^{2+}]_i$ changes, and by recording miniature EPSP (mEPSP) and firing activity from single afferent fibers of the posterior nerve.

Materials and Methods

Cell and tissue preparations. The care and use of the animals reported in this study were approved by the Animal Care and Use Committee of the local university. For most patch-clamp experiments, thin slices were obtained from the posterior semicircular canal of the frog (*Rana esculenta,* 25–30 gm body weight) by sectioning the vestibular epithelium through planes parallel to the long axis of the crista using a tissue slicer (Vibroslice, Campden Instrument, Sileby, UK), as described previously (Masetto et al., 1994), while bathing the preparation in a solution containing the following (in mM): 130.4 NaCl, 0.7 NaH_2PO_4, 3 KCl, 5.4 $MgCl_2$, 10 HEPES-NaOH, and 6 D-glucose, pH 7.25, 275 mOsm/kg. In experiments using perforated-patch recording (see below), hair cells were acutely dissociated as described in Perin et al. (2001) after incubating the ampulla of the semicircular canal in HBSS supplemented with trypsin (5 mg/ml) and EDTA (2 mg/ml) for 20 min. Whole crista slices or isolated hair cells were plated under the microscope and continuously superfused at 2 ml/min with a solution containing the following (in mM): 135 NaCl, 0.7 NaH_2PO_4, 3 KCl, 1.8 $CaCl_2$, 10 HEPES-NaOH, and 6 D-glucose, pH 7.25, 275 mOsm/kg.

Patch-clamp recordings and drug delivery. Conventional whole-cell patch-clamp recordings were made under visual control using 1.5 mm outer diameter glass capillaries (PG150T-10 Harvard Apparatus, Edenbridge, UK). Patch pipettes were filled either with a CsCl-based intracellular solution containing the following (in mM): 103 CsCl, 20 TEA Cl, 2 $MgCl_2$, 1 ATP K^+ salt, 0.1 GTP Na^+ salt, 5 HEPES-CsOH, and 0.5 EGTA, pH 7.2, 250 mOsm/kg; or they were filled with a KCl-based solution containing the following (in mM): 115 KCl, 2 $MgCl_2$, 1 ATP K^+ salt, 0.1 GTP Na^+ salt, 5 HEPES-KOH, and 0.5 EGTA, pH 7.2, 250 mOsm/kg. For perforated patch recordings, pipettes were front-filled with a KCl-based solution containing the following (in mM): 75 KCl, 2 $MgCl_2$, 30 K_2SO_4, 10 HEPES-KOH, and 5 NaCl, pH 7.25, 250 mOsm/kg and back-filled with the same solution supplemented with amphotericin B (1 mg/ml) diluted from a stock solution (50 mg amphotericin/ml DMSO) prepared daily. Electrical signals were measured either with a List EPC-7 (Heka, Lambrecht, Germany) or with an Optopatch patch-clamp amplifier (Cairn Research, Faversham, UK) by sampling current and voltage at 23 kHz using a standard laboratory interface (1401Plus; Cambridge Electronic Design, Cambridge, UK) controlled by customized software. Drugs were applied using a multibarrel pipette system with a common outlet gated by solenoid valves (ValveMate-2; Dagan, Minneapolis, MN) under software control. Typical delivery delays were in the range of 1 to 5 sec. Solutions containing ryanodine (Calbiochem, La Jolla, CA) were continuously superfused for 8–10 min before switching back to the control bathing medium.

Capacitance measurements. Capacitance measurements were made in dissociated hair cells from the frog crista, in the perforated-patch configuration. Whole-cell capacitance (C_m) was monitored by setting the Optopatch amplifier in the track-in mode (Johnson et al., 2002). After a partial manual compensation of series resistance (R_s) and C_m, 40 mV peak-to-peak voltage sinusoids at 1.5 kHz were superimposed on a nominal holding voltage of −80 mV, and R_s and C_m controls were manually adjusted to minimize the sinusoidal component of the whole-cell current. At this point, the built-in lock-in amplifier was turned on, the phase was manually optimized, and capacitance and resistance dithering circuits were activated to calibrate the system. R_s values typically ranged from 5 to 12 MOhm; cells displaying higher R_s values were discarded. The track-in feedback circuit was then switched on, and its gain was gradually increased to its highest stable value (usually 50). C_m was recorded for 60 sec at −80 mV to monitor baseline stability. Cells were stimulated by 50–1000 msec depolarizing commands to −20 mV, during which the lock-in signals were gated out. C_m traces were recorded at 1 kHz and filtered online at 150 Hz. When necessary, they were also filtered offline using a three-point boxcar filter.

Ca^{2+} fluorescence imaging. For fluorescence imaging of intracellular Ca^{2+}, cells were loaded through the patch pipette with membrane-impermeant Oregon Green 488 BAPTA-1 (Molecular Probes, Eugene, OR) dissolved at a concentration of 50 μM in the intracellular solutions described above. When performing perforated-patch recording, cells were incubated for 40 min at room temperature in the superfusion medium supplemented with the AM-ester derivative of the same dye, in the presence of Pluronic F-127 (0.01% w/v) and sulfinpyrazone (250 μM). A narrow range of excitation wavelengths was selected around the absorption maximum of the dye using a fast-switching monochromator (Polychrome IV; TILL Photonics, Martinsried, Germany) and directed onto the sample by a dichromatic beam splitter (500dcrxu; Chroma Technology, Brattleboro, VT). Oregon Green fluorescence emission, collected with a 60× objective lens (0.9 numerical aperture, LUMPlanFl W.I.; Olympus, Tokyo, Japan), was selected at 535 nm using a narrow-band interference filter (D535/40m; Chroma) to form fluorescence images on a scientific-grade CCD camera (SensiCam; PCO Computer Optics, Kelheim, Germany). The camera sensor was binned 4 × 4 to produce 320 × 240 pixel images (12 bits per pixel) that were acquired at rates of 30 per second and recorded in real time to the random access memory of a host personal computer. Imaging and electrophysiology data were synchronized by sampling the frame-valid (FVAL) signal of the CCD camera, as described in Mammano et al. (1999). Oregon Green fluorescence changes, signaling Ca^{2+} binding to the dye, were quantified as $\Delta F/F_0 \equiv [F(t) - F_0]/F_0$, where $F(t)$ is fluorescence intensity at time t and F_0 is prestimulus intensity averaged over a suitable number of frames (generally 20; Canepari and Mammano, 1999). For some experiments, whole crista slices were incubated with the membrane permeable AM-ester derivative of fura-2 (10 μM) for 30 min at room temperature in the presence of Pluronic F-127 (0.01% w/v) and sulfinpyrazone (250 μM). Slices were then left in the superfusion stream for at least 10 min before recording. Fura-2 fluorescence was excited alternatively at 360 nm (isosbestic point) and 380 nm by triggering the monochromator with the FVAL signal of the CCD camera. Fluorescence emission was selected at 510 nm using a narrow-band interference filter (D510/40m; Chroma). Fura-2 data are shown either as uncalibrated 360:380 nm ratios (R) or as ratio changes ($\Delta R = R - R_0$), where R_0 is the prestimulus ratio and R is ratio at time t. All data were analyzed offline using the Matlab 6.1 software package (MathWorks, Natick, MA).

Recording of single-fiber afferent activity from the intact frog labyrinth. Details of recording and offline analysis procedures used in this type of experiments have been extensively described in previous papers (Rossi et al., 1994; 1996). Briefly, the posterior ampulla and its nerve were exposed in the frog head, and the labyrinth, protected by its bone, was isolated, transferred to a small Perspex chamber (5 ml volume) and mounted at the center of a small turntable, orienting the posterior canal in the plane of table rotation. The turntable assembly was equipped with a custom-made miniaturized microelectrode amplifier (0–5 kHz bandwidth), and the recorded potentials were transferred through low noise sliding contacts to the oscilloscope and tape recorder. The turntable was driven by a servo motor controlled by a function generator. During mechanical stimulation, the canal was subjected to sinusoidal velocity stimuli at 0.1 Hz, resulting in acceleration peaks of 12.5 deg/sec^2. Intracellular recordings were obtained both at rest and during rotation using sharp glass microelectrodes filled with 3 M KCl, inserted into the posterior nerve close to the synapse (~500 μm). The Ringer solution was composed on the following (in mM): 120 NaCl, 2.5 KCl, 2 $CaCl_2$, 1 $MgCl_2$, 5 Tris-HCl, and 5 glucose, pH 7.2, osmolality 248 mOsm/kg. To maintain osmolality when adding caffeine, the concentration of NaCl was appropriately reduced. After recording spontaneous and mechanically evoked sensory discharge in control conditions, the liquid content of the chamber was removed with a pipette, and test solutions were gently infused with a syringe while recording

from the selected fiber. In control and test experiments the mean resting activity was evaluated over 15 sec periods; the evoked discharge was computed as the difference between the excitatory and the inhibitory responses during a cycle of sinusoidal canal rotation.

Quantal analysis. Before evaluating mEPSP properties, action potentials (APs) were automatically counted and digitally subtracted. In general, mEPSPs occurred at high frequency (>100 per second), which hampered a direct evaluation of event number and size. To circumvent this problem, mEPSP signals were routinely sharpened by a digital Wiener filter before being automatically counted. The filter was designed using the mEPSP waveform deduced from the autoregressive fit (fifth order) to the autocorrelation of the signal. This procedure made it possible to obtain time-varying estimates of mEPSP amplitude and rate of occurrence. To evaluate changes in mEPSP size and waveform, a multistage AC trigger routine was first used to detect the events; mEPSPs were subsequently aligned after saving a record on disk for each counted event. Twenty to 50 records containing isolated events were selected and averaged, and the averaged mEPSP waveform was fitted using a modified γ-distribution function:

$$w(t) = h \times (\beta t)^{\gamma} \times \exp(-\beta t)/\Gamma(\gamma+1),$$

where h is a size factor (height, mV), β (per second) defines the time scale, Γ indicates Euler's γ-function (i.e., $\Gamma(\gamma + 1) = \int_0^{\infty} t_v^{\gamma} \exp(-t)dt$) and the parameter γ determines the shape of $w(t)$, from a single exponential ($\gamma = 0$) to a near-Gaussian shape, for $\gamma > 10$. Thus, the gamma function can describe most waveforms produced by cable distortions of elementary electrical signals. The time to peak is $\tau = \gamma/\beta$, and the peak amplitude is:

$$V_p = h \times w(\tau) = h\gamma^{\gamma} \exp(-\gamma)/\Gamma(\gamma+1).$$

For additional details on this use of the gamma function, see Rossi et al. (1994). All computations were performed on data recorded using a Racal 4DS recorder (Racal Industries, Southampton, Hants, UK) and analyzed offline on a personal computer, using acquisition hardware/software by Axon Instruments (Union City, CA) and the Matlab 5 software environment (MathWorks).

All compounds were purchased from Sigma (St. Louis, MO), except where explicitly stated. Results are given as means ± SE.

Results

Spatial and temporal features of Ca^{2+} signals in patch-clamped crista hair cells

For most of the present experiments we maintained the hair cells *in situ*, in the crista

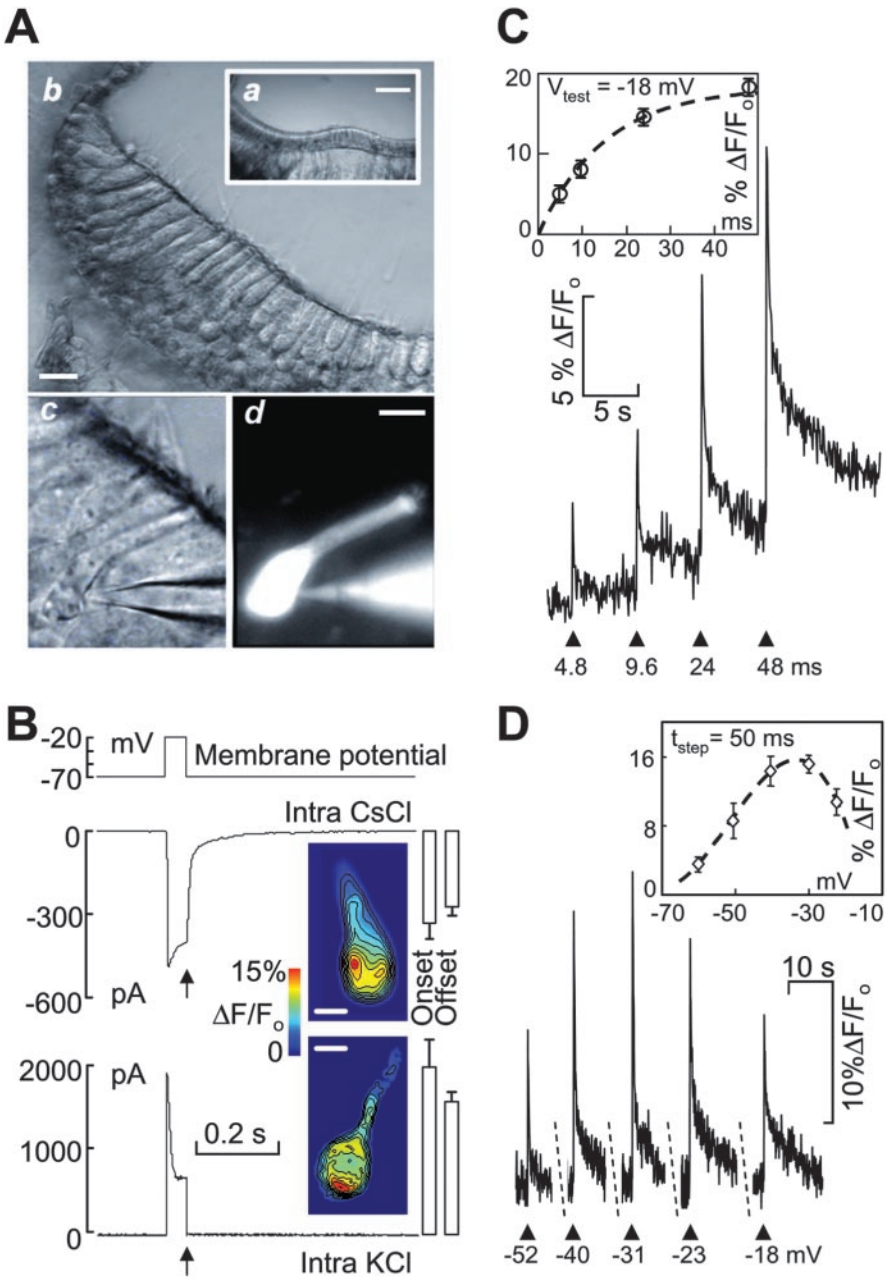

Figure 1. Spatial and temporal features of Ca^{2+} responses to depolarizations measured *in situ* from canal hair cells. *A*, Whole-cell patch-clamp recordings were performed in thin slices of the frog crista ampullaris (*a;* scale bar, 100 μm); *b*, peripheral region of the crista viewed at larger magnification (scale bar, 20 μm); *c*, hair cell contacted by a patch pipette entering from the right and containing the membrane-impermeant Ca^{2+}-selective dye Oregon Green 488 BAPTA-1 50 μM; *d*, same field as in *c*, viewed under epifluorescence illumination (scale bar, 10 μm). *B*, Whole-cell currents evoked by 50 msec depolarizations to −20 mV (top) using CsCl-based (middle) and KCl-based (bottom) intracellular solutions, respectively, for solution composition (see Materials and Methods). Inset images were recorded at the times marked by vertical arrows (end of voltage command) and color coded to highlight Ca^{2+}-dependent fluorescence changes ($\Delta F/F_o$) relative to prestimulus conditions (F_o). Contour lines (in black) superimposed on each image join points of equal fluorescence intensity to aid visualization of maximal response zones (hot spots). Scale bars, 5 μm. Bar diagrams next to images are pooled data showing current amplitude at command onset and offset (mean + SE, $n = 6$). *C*, Ca^{2+} responses elicited by four consecutive depolarization steps (arrowheads) to $V_{test} = -18$ mV for the indicated command durations. Inset, Percent fluorescence change versus command duration (mean ± SE; $n = 3$ cells in three different slices); the dashed line is a least-square fit to the data with function $f(t) = c[1 - \exp(-t/\tau)]$, where t is time (in milliseconds), $c = 18\%\ \Delta F/F_o$, and $\tau = 15$ msec. *D*, Ca^{2+} responses elicited by five consecutive steps to the indicated test potentials (arrowheads) for fixed command duration ($t_{step} = 50$ msec). Inset, Percent fluorescence change versus membrane potential (mean ± SE; $n = 6$ cells in three different slices); the dashed line is a least-squares fit to the data with function $f(V) = -0.0008V^3 - 0.1238V^2 - 5.4421V - 59.0876$, where V in membrane potential (in millivolts), peaking at −32.8 mV. Potentials were corrected for the voltage drop attributable to access resistance (17 ± 6 MΩ). Representative fluorescence traces in *C* and *D* were formed as pixel spatial averages from 2.25 μm^2 regions of interest (ROIs) encompassing the brightest hot spot of two different cells, both maintained at a holding potential of −70 mV. Experiments in *C* and *D* were performed with KCl-based intracellular solutions under whole-cell recording conditions.

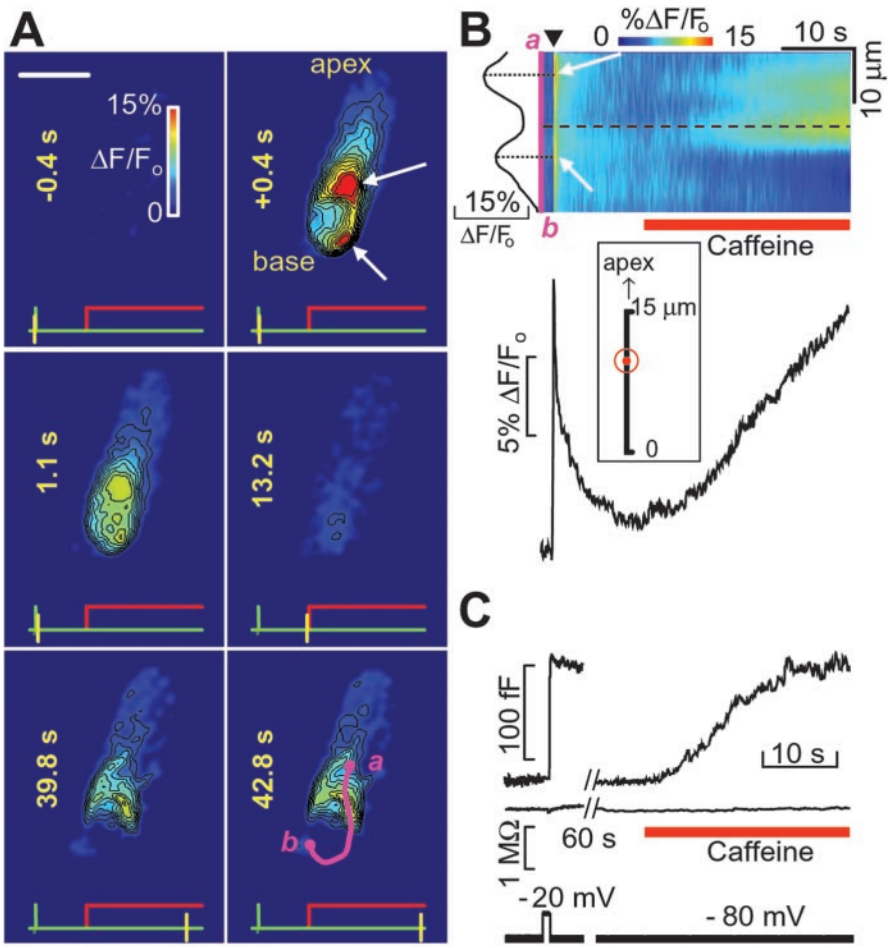

Figure 2. Ca^{2+} signals and membrane capacitance changes evoked by the application of caffeine to hair cells. *A*, Sequence of six color-coded fluorescence images of a hair cell captured at the times indicated on each frame, relative to the onset of a 50 msec depolarizing step to −20 mV; white arrows on the second frame indicate two depolarization-induced hot spots, located just above and below the nucleus, respectively. Caffeine (10 mM) was applied after capturing the fourth of the displayed frames, and maintained throughout the rest of the recording. At the bottom of each frame: the green trace is voltage command; the red trace is caffeine pulse; and the yellow cursor marks frame timing. Scale bar, 10 µm. *B*, top, Pseudo-line-scan representation of fluorescence intensity changes from the cell in *A*. Abscissas represent time and ordinates are distance along the purple line (*a*–*b*), shown on the last frame in *A*. The arrowhead marks the onset of the 50 msec voltage command, whereas white arrows point to the same two hot spots shown in *A*. In this and subsequent figures, the hilly $\Delta F/F_o$ profile to the left of the line scan image plots pixel intensity profile along the *a*–*b* line at the offset of the depolarization; relative maxima (dotted lines) correspond to hot spot locations. *B*, bottom, Fluorescence trace measured at the site of maximal caffeine-induced response (dashed line), located between the two hot spots. Inset, Average distance of maximal caffeine-induced release site from the cell base [mean (dot) ± SE (circle), $n = 6$ cells in four slices]. *C*, Cell membrane capacitance (C_m, top) and series resistance (R_s, middle) measured from a different hair cell under perforated-patch conditions. The voltage stimulus (bottom) was a 1 sec command to −20 mV from a holding potential of −80 mV. A 40 mV peak-to-peak sinusoid at 1 kHz (displayed as a black rectangle over the voltage trace) was superimposed on the holding potential (see Materials and Methods). After recovery of baseline capacitance, 0.5 mM caffeine (red bar) was applied to the same cell, producing a graded ΔC_m signal.

ampullaris (Fig. 1*A*, top), using a thin slice preparation of the frog semicircular canal (Masetto et al., 1994). Individual cells in the slice were patch-clamped under visual control and loaded with the membrane impermeant form of a Ca^{2+} selective dye (Oregon Green 488 BAPTA-1, 50 µM) through the patch pipette (Fig. 1*A*, bottom). Depolarizing the hair cell to −20 mV from a holding potential of −70 mV (Fig. 1*B*, top) evoked focal transient increase of the $[Ca^{2+}]_i$, as reported by the fluorescence intensity change, $\Delta F/F_o$, of the Ca^{2+} indicator. Both with Cs^+ and with K^+ as the main cation in the pipette solution, Ca^{2+} signals were localized to hot spots at the cell synaptic pole (inset images). The use of a Cs^+-based intracellular solution permitted to estimate the size of the underlying inward Ca^{2+} current (middle) that was otherwise masked by the outward K^+ current (bottom), as documented previously in this preparation (Perin et al., 2001; Russo et al., 2001). However, because intracellular Cs^+ apparently inhibits Ca^{2+} release in ventricular myocytes (Han et al., 1994; Kaway et al., 1998) and mouse inner hair cells (Kennedy and Meech, 2002), the rest of the patch-clamp experiments reported in this study, including those obtained in perforated patch conditions, were performed using KCl-based intracellular solutions.

The amplitude of the $[Ca^{2+}]_i$ transients at the brightest cell hot spot was a monotonically increasing function of command duration (Fig. 1*C*), saturating above 50 msec ($n = 3$), and a bell-shaped function of voltage (Fig. 1*D*), peaking at −33 ± 2 mV ($n = 6$), close to the maximum of the Ca^{2+} current (Martini et al., 2000). Ca^{2+} signals were completely suppressed when Cd^{2+} (500 µM) was included in the superfusate, or when the slice was transiently bathed in Ca^{2+}-free extracellular medium, supplemented with 1 mM EGTA ($n = 4$ cells in three slices; data not shown).

Ca^{2+} signals and membrane capacitance changes evoked by application of caffeine to hair cells

Caffeine is widely recognized as an agent capable of facilitating CICR by sensitizing ryanodine receptors to Ca^{2+}, with threshold concentration around 1 mM (Verkhratsky and Shmigol, 1996). We pressure-applied caffeine to hair cells after eliciting Ca^{2+} entry with short (50 msec) depolarization steps to −20 mV (Fig. 2*A*). In these conditions, caffeine (1–10 mM) induced an increase of $[Ca^{2+}]_i$ at the cell synaptic pole. The effect of caffeine was more pronounced in club-shaped hair cells from the crista periphery. In general, the site of maximal caffeine-induced $[Ca^{2+}]_i$ increase was distinct from the hot spots induced by depolarization. To highlight these spatial relationships, we traced a line over the cell body encompassing the largest number of hot spots (purple line *a*–*b*, last frame in Fig. 2*A*). We then generated two-dimensional pseudo-line-scan images by raster-plotting color-coded $\Delta F/F_o$ signals from each pixel along this line (ordinates) versus time (abscissa), as shown in Fig. 2*B*. In the representative cell shown, the caffeine-induced $[Ca^{2+}]_i$ increase was maximal at a site (dotted line) comprised between the two brightest hot spots (white arrows). Averaging over $n = 6$ cells in three slices confirmed that the Ca^{2+}-release site was located in a perinuclear region (inset) 9.7 ± 0.8 µm [mean (dot) ± SE (circle)] from the cell base.

Being intrinsically limited by diffraction, conventional fluorescence microscopy cannot explore the cytoplasm region within 40 nm of the plasma membrane, which is critical for most Ca^{2+}-dependent processes occurring at presynaptic active zones (Ne-

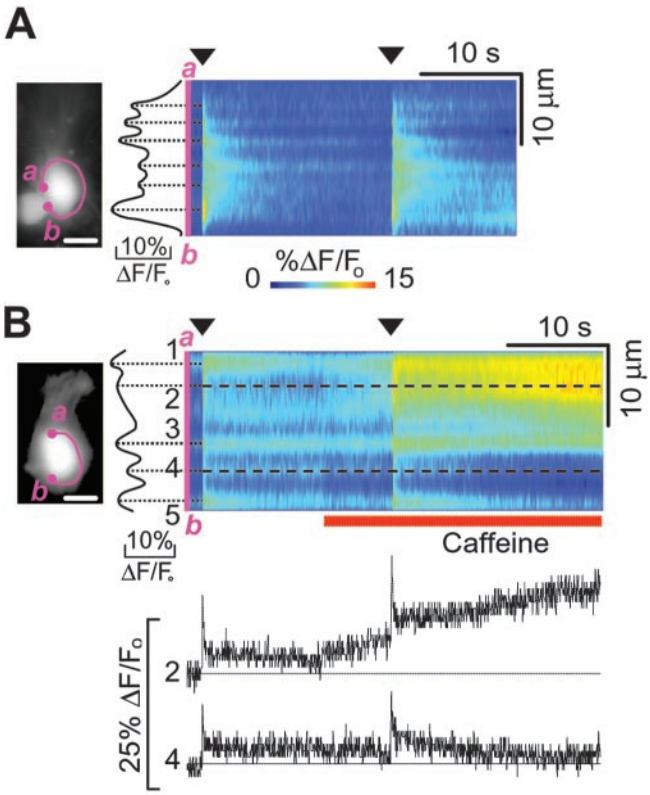

Figure 3. Caffeine increases Ca^{2+} responses at selected hot spots. *A*, Ca^{2+} responses elicited by two consecutive 50 msec depolarizations to −20 mV (arrowheads) spaced by 20 sec; holding potential, −70 mV. *B*, top, In a different cell, the second voltage pulse was preceded by application of 1 mM caffeine (red bar). *B*, bottom, Fluorescence traces corresponding to hot spots 2 and 4 (dotted lines). Note the strong potentiation induced by caffeine at hot spot 2, but not at hot spot 4.

her, 1998). As a functional probe for these processes, we used capacitance measurements in perforated-patch conditions. These measurements are widely used to monitor exocytosis, because vesicle fusion increases cell surface, hence capacitance (for review, see Gillis 1995). Fig. 2*C* shows that applying caffeine at 0.5 mM concentration (red bar) induced a gradual C_m increase of size comparable to the ΔC_m step evoked by depolarizing the hair cell to −20 mV for 1 sec. The maximal rate of change of capacitance during caffeine application was $\Delta C_m/\Delta t = 6.5 \pm 1.3$ fF (femtofarad) per second ($n = 3$). The corresponding rate $\Delta F/F_o/\Delta t$ for the caffeine-evoked increase was 0.53 ± 0.12% per second ($n = 6$). To aid comparison, we tentatively normalized each rate by the amplitude of the average response evoked by a 50 msec depolarization to −20 mV (~28 fF and 15%, respectively). This procedure yielded relative rate constants of 0.233 ± 0.047 per second and 0.035 ± 0.008 per second, respectively, for the ΔC_m and $\Delta F/F_o$ increase evoked by caffeine. As is well known, compared with the free $[Ca^{2+}]_i$ signals sensed by synaptic vesicles, $\Delta F/F_o$ signals are substantially low-pass-filtered (in time) and compressed (in amplitude) because of diffusion and buffering by the fluorescent probe (Canepari and Mammano, 1999). Therefore, these simple computations suggest that the kinetics of ΔC_m signals evoked by caffeine reflect the underlying slow $[Ca^{2+}]_i$ dynamics. However, clear caffeine-induced ΔC_m responses were observed in 3 of 35 experiments. This corresponds to about half the fraction of cells, which, in response to caffeine, generated sizable $\Delta F/F_o$ signals. Thus, competition between exocytosis and endocytosis may have also played a role by slowing down, or even occasionally canceling out altogether, the net C_m change attributable to caffeine application.

Caffeine effects on Ca^{2+} responses at active zones

ΔC_m measurements provide information on the cumulative effect of vesicle fusion. However, each hair cell in the frog semicircular canal makes several (up to 20) distinct afferent contacts (Lysakowski, 1996). These may in principle differ functionally from each other, as found, for instance, for afferent contacts of inner hair cells in the mammalian cochlea (Merchan-Perez and Liberman, 1996).

To investigate the possibility that different presynaptic active zones are regulated differently by CICR, we tested the effect of caffeine on Ca^{2+} signals evoked by depolarization under whole-cell patch-clamp recording conditions. In double pulse protocols, pairs of 50 msec depolarizations to −20 mV, separated by an interpulse interval of 20 sec, evoked Ca^{2+} hot spot signals of similar amplitude and time course after each pulse (Fig. 3*A*). When the second depolarization was preceded by the application of caffeine (Fig. 3*B*, red bar), responses measured close to the cell base (e.g., trace number 4) were enhanced less than those at some distance from it (e.g., trace n.2). On average, Ca^{2+} fluorescence changes measured 5 sec after the onset of the second depolarization increased to 258 ± 43% of control ($n = 6$ cells in three slices, $p < 0.01$) at the hot spot undergoing maximal potentiation, which was generally close to the site of maximal Ca^{2+} release evoked by caffeine (Fig. 2*B*, inset).

Effects of ryanodine on hair cell Ca^{2+} signals and exocytosis

In these experiments, recordings were obtained using the perforated-patch method (Rae et al., 1991). Longer depolarization commands were applied to hair cells to test whether, in these conditions, CICR could be elicited by voltage-dependent Ca^{2+} inflow, and blocked by ryanodine. As is well known, CICR is inhibited by incubation with ryanodine at concentrations >20 µM (Sutko et al., 1997) for several minutes. In a number of controls, both ΔC_m and Ca^{2+} fluorescence changes evoked by depolarization remained stable for the duration of the experiment (20–40 min), provided that successive voltage commands were spaced by ≥40 sec.

Figure 4*A* shows the time course of Ca^{2+} signals evoked by 500 msec commands to −20 mV and averaged over the whole synaptic pole: circles and triangles give normalized amplitudes of the Ca^{2+} responses in a control cell, and in a second cell exposed to 40 µM ryanodine for 8 min (gray bar), respectively. Representative traces and pseudo color $\Delta F/F_o$ images of these two hair cells, captured at time points marked c_1 and c_2 (solid lines, control) and r_1, r_2, and r_3 (dotted lines, ryanodine) are also displayed showing that, within 20 min, ryanodine strongly inhibited Ca^{2+} responses (the effects of ryanodine are reputedly irreversible). However, a small remnant of the initial Ca^{2+} signal could still be detected at selected sites (inset image r_3) also when the spatially averaged response seemed virtually flat (e.g., trace r_3). ΔC_m traces obtained from the same two cells are plotted in Figure 4*B*, with identical line-style coding. In $n = 3$ experiments, the mean percent changes between c_1 and c_2 (control) and r_1 and r_3 (ryanodine) for ΔC_m responses were 1 ± 8% and 58 ± 2%, respectively. The corresponding figures for Ca^{2+} were 11 ± 20% and 85 ± 21%. As shown in Figure 4*B*, incubation with ryanodine decreased, but did not abolish, the exocytotic response to depolarization. This is consistent with the persistence, in the presence of ryanodine, of residual Ca^{2+} signals attributable to voltage-gated Ca^{2+} entry, as noted above, which were probably confined to the

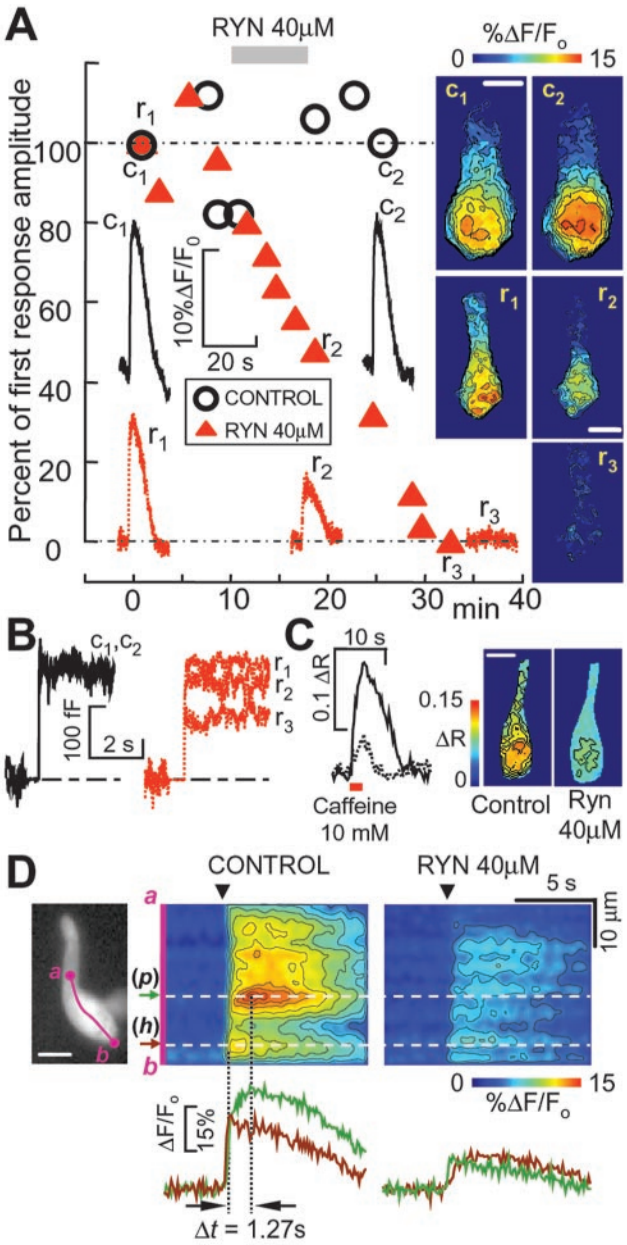

Figure 4. Effect of ryanodine on Ca^{2+} signals and exocytosis. *A,* Time course of ryanodine (RYN) effects on Ca^{2+} responses evoked by 500 msec depolarizations to −20 mV measured from isolated hair cells in perforated-patch conditions; holding potential, −80 mV. In control experiments (open circles), responses were usually stable for at least 25 min. The application of 40 μM ryanodine (RYN) for 8 min (gray bar) caused a steady and irreversible decline of Ca^{2+} responses (filled triangles, different cell). Symbols represent peak Ca^{2+} responses averaged over a 64 μm^2 ROI superimposed on the cell synaptic pole, normalized to the first recording. Representative sample traces corresponding to labeled symbols are shown (c_1 and c_2, control; r_1, r_2, and r_3, ryanodine), together with corresponding $\Delta F/F_o$ cell images recorded at response peak times and color coded to highlight Ca^{2+}-dependent fluorescence changes relative to prestimulus conditions (as in Fig. 2*A*). *B,* Effects of ryanodine on cell capacitance: same cells, stimulation protocols, trace labels, and line styles as in *A.* In control experiments (left), ΔC_m recordings were stable for at least 25 min (overlapping traces c_1 and c_2), whereas 40 μM ryanodine (right) decreased ΔC_m (traces r_1, r_2, and r_3), although less markedly than the corresponding Ca^{2+} responses in *A. C,* Effect of transient caffeine application (10 mM, 2.5 sec, red bar) on a hair cell in a whole crista slice loaded with fura-2 AM, before (solid line and left image) and after a 6 min incubation with 40 μM ryanodine (dotted line and right image). Responses are given as uncalibrated 360/380 nm fura-2 ratio changes $\Delta R = R - R_o$, where R_o is prestimulus ratio (see Materials and Methods). Traces represent the time course of pixel spatial averages computed over the whole synaptic pole. *D,* Ryanodine affects Ca^{2+} responses differently in different subcellular regions. *D,* left, Hair cell loaded with the AM ester of Oregon Green under perforated patch recording conditions (scale bar, 10 μm); the tip of the patch pipette, entering from the right, hosts an internally sealed ω-shaped fraction of the plasma membrane and related fluorescent cytoplasm. *D,* middle, In control conditions, 500 msec depolarization to −20 mV (arrowhead) evoked an immediate Ca^{2+} response at (h), near the bottom of the cell, whereas the larger responses at (p) displayed an additional slower phase, peaking 1.27 sec later. *D,* right, Perfusion of ryanodine 40 μM depressed Ca^{2+} responses throughout the cell, but relatively more at (p), which is hence functionally identified as a preferential site for CICR, consistent with the results illustrated in Figures 2 and 3.

subplasmalemma region by powerful cytoplasmic buffers (Edmonds et al., 2000); but nonetheless sufficed to evoked the ΔC_m signals in Figure 4*B*.

To test whether ryanodine calcium-loaded the cell, a number of controls were performed using the AM ester of fura-2 to image calcium in whole crista slices. In $n = 46$ hair cells of three different slices, the mean ± SD of the uncalibrated fura-2 ratio before and 10 min after ryanodine were $r = 0.59 \pm 0.06$ and $r = 0.64 \pm 0.06$, respectively (see Materials and Methods). This difference is not statistically significant, implying that resting cytosolic calcium levels were not affected by exposure to ryanodine.

The same approach was used also to perform competitive experiments in fura-2-loaded slices, in which ~18% of the hair cells responded to caffeine also in the absence of depolarization. In Figure 4*C,* representative responses to the transient application of caffeine (10 mM, 2.5 sec, red bar) before (solid line and left image) and after 6 min incubation with 40 μM ryanodine (dotted line and right image) are compared. Combined with the calcium-load controls, these results indicate that: (1) ryanodine and caffeine acted on a common intracellular Ca^{2+} pool and (2) the effects of ryanodine were mediated by interference with CICR and did not involve, for instance, calcium-dependent inactivation of the calcium current.

Ca^{2+} signals evoked by 500 msec depolarizations to −20 mV under perforated-patch conditions (Fig. 4*D,* left) were highly nonuniform over the cell synaptic pole and were also differentially affected by ryanodine. In control conditions (middle), Ca^{2+} transients peaked more rapidly near the base of the cell (*b*), whereas the largest signal measured ~10 μm further up (toward the apex of the cell) developed with a slower time course and peaked with a delay $\Delta t > 1$ sec from the onset of the command. Although genuinely bimodal response were not observed, the amplitude of the slower response (dark green trace, p) exceeded by >30% the amplitude of the faster signal (brown trace, h), which is inconsistent with simple $[Ca^{2+}]_i$ diffusion from the hot spot (h) to (p). After incubation with 40 μM ryanodine for 10 min (right), Ca^{2+} signals were attenuated throughout the cell. But ryanodine also reduced the difference between the (p) and (h) responses. Consistent with the results illustrated in Figures 2 and 3, these results point to (p) as a preferential site for CICR. Results in Fig. 4*A,B,* Fig. 4*C,* and Fig. 4*D* are representative of two, two, and four other experiments, respectively.

Effects of ryanodine on Ca^{2+} responses to short (50 msec) depolarizations were also tested using the perforated-patch method in whole crista slices. Under these conditions, Ca^{2+} signals remained confined to the vicinity of the hot spots. Nonetheless in two of two experiments fura-2 ratio signals ΔR, averaged over the cell synaptic pole to encompass the majority of the hot spots, were reduced by >30% after incubation with 40 μM ryanodine for 12 min (data not shown).

←

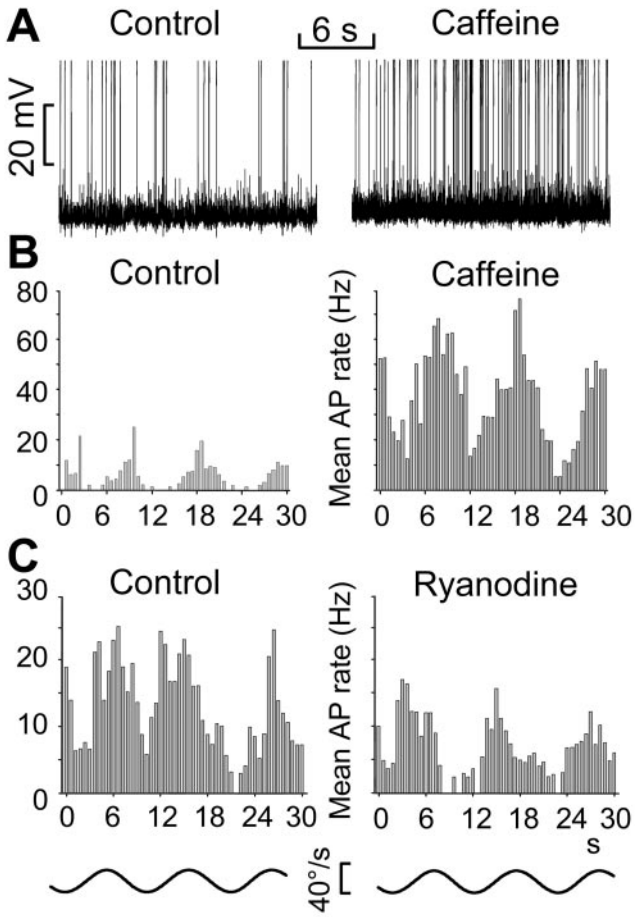

Figure 5. Effect of caffeine and ryanodine on afferent activity measured in the intact labyrinth from single fibers of the vestibular nerve. *A,* Spontaneous activity recorded from a posterior canal spiking unit, in control solution (left) and in the presence of 20 mM caffeine (right); APs are truncated. *B,* AP frequency histograms from a single unit during canal rotation with sinusoidally varying velocity (0.1 Hz; peak acceleration, 12.5 deg/sec^2) in control solution (left) and in the presence of 20 mM caffeine (right) (bin width, 0.6 sec). *C,* AP frequency histograms showing the inhibitory effect of 1 mM ryanodine on the evoked discharge. Turntable angular velocity is illustrated at the bottom. Caffeine and ryanodine concentrations are nominal. The actual concentrations sensed by the hair cells in this semi-intact preparation remain undetermined because of the presence of several diffusion barriers.

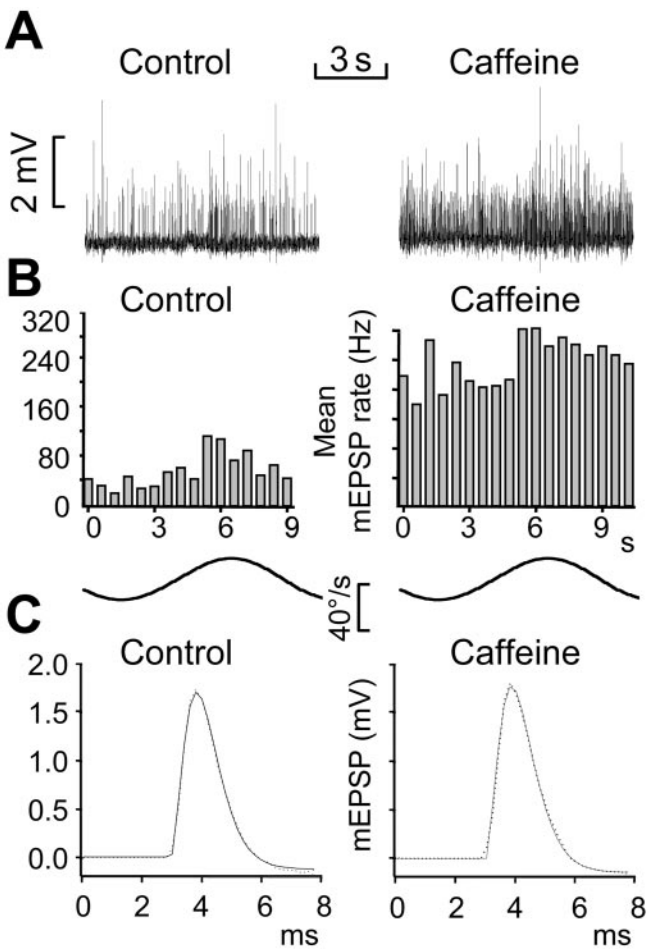

Figure 6. Caffeine affects the frequency but not the shape of mEPSPs. Recordings of mEPSP evoked activity (*A*) and the corresponding frequency histogram (*B*) in a fiber that did not fire APs (bin width, 0.6 sec), showing a clear potentiation by 20 mM caffeine (right) relative to control responses (left). Turntable angular velocity is illustrated under the histograms. *C,* Analytical fits by modified γ-distribution functions (continuous lines) to the average of 20 mEPSPs (dotted lines) in control conditions (left) and after application of caffeine (right) at a nominal concentration of 20 mM. For fit parameters, see text.

Effect of caffeine and ryanodine on single-fiber afferent activity

To investigate the postsynaptic counterpart of Ca^{2+} store activation and inhibition, recordings were obtained from single posterior canal afferent fibers in an intact labyrinth preparation that was either kept at rest or subjected to periodic mechanical stimuli.

Figure 5 shows APs recorded from a posterior canal unit before (left) and after (right) exposure to caffeine or ryanodine. Caffeine (Fig. 5*A,B;* nominal concentration, 20 mM) dramatically increased spontaneous activity (Fig. 5*A*), as well as mean AP frequency during canal rotation with variable angular velocity (Fig. 5*B*). In the presence of caffeine, the frequencies of spontaneous and mechanically evoked APs increased to 372 ± 120% ($n = 5$) and 237 ± 151% ($n = 3$) of control, respectively. Although the differences are not significant, it appears that caffeine may be more effective in modulating spontaneous than mechanically evoked release. Opposite effects were produced by incubation with ryanodine for 10 min (Fig. 5*C,* nominal concentration 1 mM). In the presence of ryanodine, the frequencies of spontaneous and mechanically evoked APs decreased to 65 ± 6% ($n = 3$) and 40 ± 10% ($n = 2$) of the control, respectively (note different ordinates scales in Fig. 5*B* and 5*C*).

Nominal drug concentrations in these experiments exceeded those applied to crista slices or isolated hair cells. Actual concentrations sensed by the hair cells in the labyrinth remain undetermined, but were undoubtedly smaller than nominal values because of the presence of several diffusion barriers.

Quantal analysis of caffeine and ryanodine effects

Caffeine (20 mM) strongly increased the frequency of both spontaneous (238 ± 38% of control, $n = 7$) and mechanically evoked mEPSPs (230 ± 47% of control, $n = 2$) (Fig. 6*A,B*); conversely, in the presence of ryanodine (1 mM), the resting and mechanically evoked mEPSP frequency decreased to ~58 ± 12% and 59 ± 32% of the control, respectively ($n = 3$) (Fig. 7*A,B*). Neither drug altered mEPSP amplitude or time course. For caffeine, this is exemplified in Figure 6*C,* which plots fits to averaged mEPSPs ($n = 20$, dotted lines) with modified γ distribution functions (continuous lines). In this unit, the parameters of the γ function in control ($\gamma = 2.94$; $\beta = 2.88$ kHz; time to peak, 1.02 msec; peak value, 1.83 mV) were nearly identical to those in the presence of

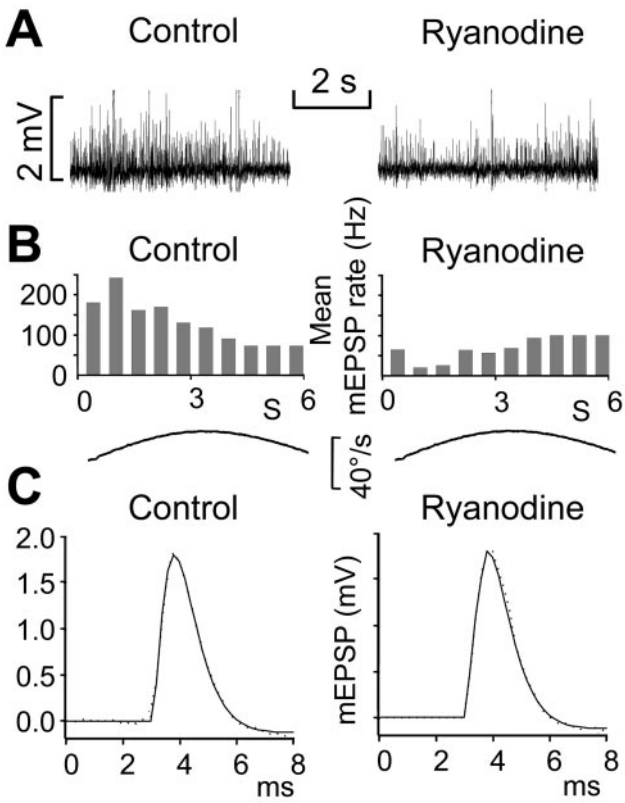

Figure 7. Ryanodine reduces the discharge of mEPSPs but not their size. Recordings (*A*) and frequency histograms (*B*) of mEPSPs during sinusoidal canal rotation (bin width, 0.6 sec) in control (left) and in 1 mM ryanodine (right). A silent unit was selected to simplify data analysis. *C*, γ distribution fit (continuous lines) to the average of 25 mEPSPs (dotted lines) to show similar shape and unvaried amplitude before and after ryanodine application. For fit parameters, see text.

the drug ($\gamma = 3.02$; $\beta = 2.86$ kHz, time to peak, 1.05 msec; peak value, 1.90 mV).

Applying the same analysis to the ryanodine experiments (Fig. 7*A*,*B*) yielded the averaged mEPSPs ($n = 25$, dotted lines) and the γ function fit (continuous lines) displayed in Figure 7*C*. Also in this case, the waveform parameters in control ($\gamma = 1.88$; $\beta = 2.27$ kHz; time to peak, 0.83 msec; peak value, 1.94 mV) and under ryanodine treatment ($\gamma = 1.96$; $\beta = 2.22$ kHz; time to peak, 0.88 msec, peak value, 1.85 mV) were nearly identical.

To investigate further the effects of caffeine and ryanodine on synaptic release, histograms of mEPSP sizes acquired before and after the application of the drugs were compared. In agreement with previous results (Rossi et al., 1994), the size distributions became multimodal when mEPSP frequency increased to high levels (>100 per second), presumably because of the difficulty in resolving the occurrence of multiple events over the rise-time of a single mEPSP; however, when the recordings were sharpened (see Materials and Methods), so that the duration of a single mEPSP became shorter than the average interval between events, all histograms reverted to a unimodal shape (data not shown; for a detailed analysis of this aspect, see Rossi et al., 1994); this, together with the observation that spike interval histograms were generally fitted well by single exponentials (data not shown), suggests that correlated, synchronous release is not a major feature of this system.

Discussion

In the present experiments, the effects of interfering with store-operated Ca^{2+} release on afferent synaptic activity were investigated using simultaneous whole-cell capacitance measurements and fluorescence imaging of intracellular Ca^{2+} from presynaptic hair cells of frog crista ampullaris (Fig. 1). These measurements were complemented by recording the activity of single afferent fibers in a semi-intact preparation of the frog labyrinth either at rest or subjected to periodic mechanical stimuli. Our results clearly indicate that CICR from caffeine- and ryanodine-sensitive stores participates in the generation of the Ca^{2+} signals evoked by depolarization in the hair cell, and contributes to shaping afferent signaling.

Presynaptic Ca^{2+} stores in vestibular hair cells

Ca^{2+}-signals evoked by caffeine were maximal in a subcellular zone (probably perinuclear), located ~10 μm from the hair cell base (Fig. 2*A*,*B*). Caffeine also produced a sizable increase in membrane capacitance (ΔC_m) that, signaling exocytosis, developed with a time course that reflected the dynamics of the underlying Ca^{2+} response (Fig. 2*B*,*C*). Consistent with these results, the suppressive effect of ryanodine on Ca^{2+} signals (Fig. 4*A*) was maximal over the same zone (Fig. 4*C*,*D*), which is dense in afferent synaptic terminals (Lysakowski, 1996). However, residual ΔC_m signal evoked by depolarization were still detectable after treatment with ryanodine (Fig. 4*B*). Competitive experiments performed in whole crista slices confirmed that caffeine and ryanodine acted on a common Ca^{2+} pool (Fig. 4*C*).

Recently, electron tomography reconstructions of hair cell presynaptic terminals revealed releasable vesicles as far as 800 nm from the synaptic body (Lenzi et al., 2002) that has long been considered responsible for the translocation of vesicles to the active zone. Current evidence indicates instead that the synaptic body may serve to facilitate multivesicular release by compound exocytosis (Parsons and Sterling, 2003). Thus, a possible implication for the results shown in Figure 4i is that both voltage-gated Ca^{2+} channels and CICR are involved in the exocytosis of transmitter at the hair cell cytoneural junction. For instance, ryanodine may have interfered with Ca^{2+} stores that influence vesicle availability and/or fusion, whereas residual Ca^{2+} signals attributable to voltage-gated Ca^{2+} entry (e.g., image r_3 in Fig. 4*A*), probably confined to the subplasmalemma region by powerful cytoplasmic buffers (Edmonds et al., 2000), sufficed to generate persistent ΔC_m signals (e.g., trace r_3 in Fig. 4*B*).

With regard to the general properties of the release mechanism in this system (Figs. 5*A*, 6*A*, 7*A*), analysis of mEPSP sizes confirms that the distributions can be made unimodal provided the mEPSP waveform is adequately shortened by appropriate filtering (Rossi et al., 1994). In other words, release remains uncorrelated and asynchronous and the drugs used in the present experiments to modulate CICR do not promote the appearance of truly multiquantal events.

However, the number of afferent boutons contributing to our recordings prevents the detailed identification of possible bursts of correlated quantal events (multivesicular release), as described in cochlear inner hair cells (IHCs) based on recordings from single afferent boutons (Glowatzki and Fuchs, 2002). A collateral aspect regards simple synchronization: fast activation (in the kilohertz range) of the synapse investigated in this study is expected to yield synchronization levels reminiscent of those described at the IHC synapse. But because the vestibular synapse responds to much lower rotation frequencies (see below), multiquantal re-

lease is unlikely to play any significant role in this system (Rossi et al., 1994).

Interference with presynaptic Ca^{2+} stores alters afferent signaling: a role for IP_3?

Caffeine and ryanodine affected also the activity of single afferent fibers in the intact semicircular canal (Figs. 5, 6, 7), confirming the results obtained from presynaptic hair cells *in vitro*. In particular, caffeine significantly increased nerve fiber activity, whereas ryanodine significantly decreased it (Fig. 5). In the presence of either drug, mEPSP waveforms were indistinguishable from controls (Figs. 6 and 7), indicating that caffeine and ryanodine acted at the presynaptic level, i.e., on the hair cell. Positive modulation by caffeine and negative modulation by ryanodine indicate that CICR plays an important role in this system, amplifying Ca^{2+} signals because of Ca^{2+} influx across the plasma membrane, producing a cycle by cycle effect on synaptic transmission (this issue is discussed further in the previous paragraph).

Presynaptic metabotropic glutamate receptors coupled to IP_3 production have been described in frog canal hair cells (Hendricson and Guth, 2002), raising the interesting possibility of an interaction between ryanodine- and IP_3-sensitive stores at these presynaptic terminals. In our experiments, a possible contribution from IP_3-sensitive stores might have been thwarted by the application of caffeine, which in the same concentration range, activates the ryanodine receptor and inhibits the IP_3 receptor (Ehrlich et al., 1994). Additional experiments are required to explore the IP_3 pathways in these cells.

Possible implications for the effect of CICR on afferent signaling

One of the most striking results obtained by sensitizing the hair cell with caffeine was a marked prolongation of the Ca^{2+} responses evoked by depolarization at selected active zones (Fig. 3). This CICR effect may be relevant for the generation of a tonic response in afferent fibers of the vestibular nerve. Interestingly, in the present experiments, CICR was observed most frequently in club-shaped hair cells, which are contacted by tonic afferent fibers (Honrubia et al., 1989). Furthermore, Ca^{2+} signals generated by intracellular stores can modulate gene expression, linking synaptic activity to long-lasting plastic changes, as is well known for other systems (Meldolesi, 2001). In fact, in animals exposed to altered gravity conditions, vestibular hair cells have been found to exhibit synaptic plasticity (Ross, 2000).

The results of our paired-pulse experiments also suggest that afferent synapses contacting the same hair cell may undergo differential modulation by CICR in physiological conditions. Differences in the functional properties of afferent synapses, contacting the same hair cell in different regions of the plasma membrane, have been reported for cochlear inner hair cells (Merchan-Perez and Liberman 1996). Our data suggest that this may be a general property of hair cell afferent innervation in both acoustic and vestibular systems.

CICR and the frequency range of mechanical stimuli

Frog canal hair cells respond to mechanical stimuli in a frequency range between 0.01 and 10 Hz (Goldberg and Fernandez, 1975). The protocol used in our postsynaptic recordings from the intact canal was designed to stimulate the cells in the mid-lower end of the frequency spectrum, generating 0.1 Hz cycles of acceleration that periodically excited the hair cells for times on the order of seconds. Our presynaptic recordings showed that depolarizations lasting 500 msec sufficed to elicit CICR at the synaptic pole of hair cells (Fig. 4*D*). Altogether, these results strongly suggest that CICR is an important component of the Ca^{2+}-dependent release machinery of the hair cell and that endogenous modulators of the CICR process will affect afferent activity elicited by mechanical stimuli in the physiological frequency range.

References

Berridge MJ (1998) Neuronal calcium signalling. Neuron 21:13–26.

Bezprozvanny I, Bezprozvannaya S, Ehrlich BE (1994) Caffeine-induced inhibition of inositol(1,4,5)-trisphosphate-gated calcium channels from cerebellum. Mol Biol Cell 5:97–103.

Canepari M, Mammano F (1999) Imaging neuronal calcium fluorescence at high spatio-temporal resolution. J Neurosci Methods 87:1–11.

Carter AG, Vogt KE, Foster KA, Regehr WG (2002) Assessing the role of calcium-induced calcium release in short-term presynaptic plasticity at excitatory central synapses. J Neurosci 22:21–28.

Edmonds B, Reyes R, Schwaller B, Roberts WM (2000) Calretinin modifies presynaptic calcium signaling in frog saccular hair cells. Nat Neurosci 3:786–790.

Emptage NJ, Reid CA, Fine A (2001) Calcium stores in hippocampal synaptic boutons mediate short-term plasticity, store-operated Ca2+ entry, and spontaneous transmitter release. Neuron 29:197–208.

Endo M, Tanaka M, Ogawa Y (1970) Calcium induced release of calcium from the sarcoplasmic reticulum of skinned skeletal muscle fibres. Nature 228:34–36.

Evans MG, Lagostena L, Darbon P, Mammano F (2000) Cholinergic control of membrane conductance and intracellular free Ca^{2+} in outer hair cells of the guinea pig cochlea. Cell Calcium 28:195–203.

Fuchs P (2002) The synaptic physiology of cochlear hair cells. Audiol Neurootol 7:40–44.

Gillis KD (1995) Techniques for membrane capacitance measurements. In: Single channel recording, Ed 2 (Sakmann B, Neher E, eds), pp 155–198. New York: Plenum.

Glowatzki E, Fuchs PA (2002) Transmitter release at the hair cell ribbon synapse. Nat Neurosci 5:147–154.

Goldberg JM, Fernandez C (1975) Vestibular mechanisms. Annu Rev Physiol 37:129–162.

Han S, Schiefere A, Isemberg G (1994) Ca^{2+} load of guinea pig ventricular myocytes determines efficacy of brief Ca^{2+} current as trigger for Ca^{2+} release. J Physiol (Lond) 480:411–421.

Hendricson AW, Guth PS (2002) Transmitter release from *Rana pipiens* vestibular hair cells via mGluRs: a role for intracellular Ca^{++} release. Hearing Res 172:99–109.

Honrubia V, Hoffman LF, Sitko S, Schwartz IR (1989) Anatomic and physiological correlates in bullfrog vestibular nerve. J Neurophysiol 61:688–701.

Issa NP, Hudspeth AJ (1996) The entry and clearance of Ca^{2+} at individual presynaptic active zones of hair cells from the bullfrog's sacculus. Proc Natl Acad Sci USA 93:9527–9532.

Johnson SL, Thomas MV, Kros CJ (2002) Membrane capacitance measurement using patch clamp with integrated self-balancing lock-in amplifier. Pflugers Arch 443:653–663.

Kaway M, Hussain M, Orchard CH (1998) Cs^{+} inhibits spontaneous Ca^{2+} release from sarcoplasmic reticulum of skinned cardiac myocytes. Am J Physiol 275:H422–H430.

Kennedy HJ, Meech RW (2002) Fast Ca^{2+} signals at mouse inner hair cell synapse: a role for Ca^{2+}-induced Ca^{2+} release. J Physiol (Lond) 539 1:15–23.

Lenzi D, Crum J, Ellisman MH, Roberts WM (2002) Depolarisation redistributes synaptic membrane and creates a gradient of vesicles on the synaptic body at a ribbon synapse. Neuron 36:649–659.

Llano I, Gonzalez J, Caputo C, Lai FA, Blayney LM, Tan YP, Marty A (2000) Presynaptic calcium stores underlie large-amplitude miniature IPSCs and spontaneous calcium transients. Nat Neurosci 3:1256–1265.

Lysakowski A (1996) Synaptic organization of the crista ampullaris in vertebrates. Ann NY Acad Sci 781:164–182.

Mammano F, Canepari M, Capello G et al (1999) An optical recording system based on a fast CCD sensor for biological imaging. Cell Calcium 25:115–123.

Martini M, Rossi ML, Rubbini G, Rispoli G (2000) Calcium currents in hair cells isolated from semicircular canals of the frog. Biophys J 78:1240–1254.

Martini M, Rossi ML, Farinelli F, Moriondo A, Mammano F, Rispoli G

(2002) No evidence for calcium electrogenic exchanger in from semicircular canal hair cells. Eur J Neurosci 16:1–8.

Masetto S, Russo G, Prigioni I (1994) Differential expression of potassium currents by hair cells in thin slices of frog crista ampullaris. J Neurophysiol 72(1):443–455.

Meldolesi J (2001) Rapidly exchanging Ca^{2+} stores in neurons: molecular, structural and functional properties. Prog Neurobiol 65:309–338.

Meldolesi J, Pozzan T (1998) The endoplasmic reticulum Ca^{2+} store: a view from the lumen. Trends Biochem Sci 23:10–14.

Merchan-Perez A, Liberman MC (1996) Ultrastructural differences among afferent synapses on cochlear hair cells: correlations with spontaneous discharge rate. J Comp Neurol 371:208–221.

Moser T, Beutner D (2000) Kinetics of exocytosis and endocytosis at the cochlear inner hair cell afferent synapse of the mouse. Proc Natl Acad Sci USA 97:883–888.

Narita K, Akita T, Hachisuka J, Huang S, Ochi K, Kuba K (2000) Functional coupling of Ca^{2+} channels to ryanodine receptors at presynaptic terminals. Amplification of exocytosis and plasticity. J Gen Physiol 115:519–532.

Neher E (1998) Vesicle pools and Ca^{2+} microdomains: new tools for understanding their roles in neurotransmitter release. Neuron 20:389–399.

Parsons TD, Sterling P (2003) Synaptic ribbon: conveyor belt or safety belt? Neuron 37:379–382.

Parsons TD, Lenzi D, Almers W, Roberts WM (1994) Calcium-triggered exocytosis and endocytosis in an isolated presynaptic cell: capacitance measurements in saccular hair cells. Neuron 13:875–883.

Perin P, Masetto S, Martini M, Rossi ML, Rubbini G, Rispoli G, Guth P, Zucca G, Valli P (2001) Regional distribution of calcium currents in frog semicircular canal hair cells. Hearing Res 152:67–76.

Rae J, Cooper K, Gates P, Watsky M (1991) Low access resistance perforated patch recordings using amphotericin B. J Neurosci Methods 37:15–26.

Ricci AJ, Gray-Keller M, Fettiplace R (2000) Tonotopic variations of calcium signalling in turtle auditory hair cells. J Physiol (Lond) 524:423–436.

Rispoli G, Martini M, Rossi ML, Mammano F (2001) Dynamics of intracellular calcium in hair cells isolated from the semicircular canal of the frog. Cell Calcium 30:131–140.

Roberts WM, Jacobs RA, Hudspeth AJ (1990) Colocalization of ion channels involved in frequency selectivity and synaptic transmission at presynaptic active zones of hair cells. J Neurosci 10:3664–3684.

Rodriguez-Contreras A, Yamoah EN (2001) Direct measurement of single-channel Ca^{2+} currents in bullfrog hair cells reveals two distinct channel subtypes. J Physiol (Lond) 534:669–689.

Rose CR, Konnerth A (2001) Stores not just for storage: intracellular calcium release and synaptic plasticity. Neuron 31:519–522.

Ross MD (2000) Changes in ribbon synapses and rough endoplasmic reticulum of rat utricular macular hair cells in weightlessness. Acta Otolaryngol 120:490–499.

Rossi ML, Martini M, Pelucchi B, Fesce R (1994) The quantal nature of transmitter release at the cytoneural junction of the frog labyrinth. J Physiol (Lond) 478:17–35.

Rossi ML, Ferrary E, Martini A, Martini M, Pelucchi B, Bernard C, Teixeira M, Sterkers O, Fesce R (1996) The effect of clofilium, a K-channel blocker, on the electrogenic K secretion and the sensory discharge at the frog semicircular canal. Brain Res 721:174–180.

Russo G, Lelli A, Marcotti W, Prigioni I (2001) Gradients of expression of calcium and potassium currents in frog crista ampullaris. Pflugers Arch 442:814–820.

Sorrentino V (2003) Ryanodine receptor type 3: why another ryanodine receptor isoform? Front Biosci 8:D176–D182.

Sutko JL, Airey JA, Welch W, Ruest L (1997) The pharmacology of ryanodine and related compounds. Pharmacol Rev 49:53–98.

Tucker T, Fettiplace R (1995) Confocal imaging of calcium microdomains and calcium extrusion in turtle hair cells. Neuron 15:1323–1335.

Verkhratsky A, Shmigol A (1996) Calcium-induced calcium release in neurones. Cell Calcium 19:1–14.

Williams AJ (2002) Ion conduction and selectivity in the ryanodine receptor channel. Front Biosci 7:d1223–30.